Research Article | Vol. 12, No. 1 / 1 January 2021 / Biomedical Optics Express 181

Biomedical Optics EXPRESS

On-chip absorption spectroscopy enabled by graded index fiber tips

KAMALPREET K. GILL,[1,2] NICOLAS RIESEN,[1,2,3,*] CRAIG PRIEST,[1,2] NICHOLAS PHILLIPS,[1,4] BIN GUAN,[1] AND DAVID G. LANCASTER[1,2]

[1] *Future Industries Institute and STEM, University of South Australia, Mawson Lakes, SA 5095, Australia*
[2] *ARC Research Hub for Integrated Devices for End-user Analysis at Low-levels (IDEAL), UniSA STEM, University of South Australia, Mawson Lakes, SA 5095, Australia*
[3] *Institute for Photonics and Advanced Sensing and School of Physical Sciences, University of Adelaide, SA 5005, Australia*
[4] *Defence Science and Technology Group, Third Ave, Edinburgh, SA 5111, Australia*
[*] *nicolas.riesen@unisa.edu.au*

Abstract: This paper describes the design and characterization of miniaturized optofluidic devices for sensing based on integrating collimating optical fibers with custom microfluidic chips. The use of collimating graded-index fiber (GIF) tips allows for effective fiber-channel-fiber interfaces to be realized when compared with using highly-divergent standard single-mode fiber (SMF). The reduction in both beam divergence and insertion losses for the GIF configuration compared with SMF was characterized for a 10.0 mm channel. Absorption spectroscopy was demonstrated on chip for the measurement of red color dye (Ponceau 4R), and the detection of thiocyanate in water and artificial human saliva. The proposed optofluidic setup allows for absorption spectroscopy measurements to be performed with only 200 µL of solution which is an order of magnitude smaller than for standard cuvettes but provides a comparable sensitivity. The approach could be integrated into a lab-on-a-chip system that is compact and does not require free-space optics to perform absorption spectroscopy.

© 2020 Optical Society of America under the terms of the OSA Open Access Publishing Agreement

1. Introduction

Optofluidics is a rapidly growing field that emerged in the early 2000s as the disciplines of nanophotonics and microfluidics matured. It holds promise for the next generation of portable molecular detectors that will ultimately become more important in our everyday life [1,2]. Optofluidics involves the simultaneous control of fluids and optical beams and aims to integrate several optical functions into a single chip in the lab-on-a-chip approach, replacing the need for bulk free-space optics [3]. With the global microfluidics market size currently USD 15.7 billion and projected to reach USD 44.0 billion by 2025 at a compound annual growth rate of 23% and with optofluidics still being in its infancy there exists significant untapped commercial potential for such optics-enriched microfluidic devices [4]. Since most lab-on-a-chip optofluidic devices have been limited to short-term research rather than being directly integrated into user-friendly real-world products, there is a need to focus on simple, practical and cost-effective devices which balance design and real-world impact. This improves the chances of techniques and technologies being developed that can be commercialized.

One of the simpler and more practical on-chip sensing techniques is absorption spectroscopy which can be used to determine the concentration of an analyte of interest through the Beer-Lambert law, which can be expressed by:

$$A = -\log\left(\frac{I}{I_0}\right) = \varepsilon l c \tag{1}$$

#414239 https://doi.org/10.1364/BOE.414239
Journal © 2021 Received 5 Nov 2020; revised 2 Dec 2020; accepted 2 Dec 2020; published 8 Dec 2020

Biomedical Optics EXPRESS

where I and I_0 are the intensities of light transmitted in presence and absence of an analyte, respectively, ε is the molar absorptivity coefficient, l is the optical pathlength and c is the concentration of the analyte in the sample. In previous work, Priest *et al.* [5,6] reported a quartz glass microfluidic chip with a micropillar array (i.e. pillar cuvette) as an effective single-pass absorption measurement platform with only ~2 µL sample volume, but which was limited by a very short interaction length l. The literature contains an increasing number of reports which propose optical detection methods that mitigate the problem of short path length, including cavity-enhanced absorption spectroscopy (CEAS) [7,8], and cavity ring-down spectroscopy (CRDS) [9,10]. These optical detection methods have their own advantages and limitations in terms of simplicity, sensitivity and cost. The simplest technique of single-pass absorption spectroscopy is usually limited to short interaction lengths (~mm's) due to the typical divergence of the beams coming from standard fibers or laser-written waveguides which limit the possible channel length because of the increased coupling losses [11].

In this paper we make significant inroads into increasing the interaction length for single-pass absorption spectroscopy by using lensed graded-index fiber (GIF) tips. GIF tips have found significant use in recent years in optical coherence tomography (OCT) biomedical imaging and micro-electromechanical system (MEMs) applications but have only seen limited use outside of these fields [12–15]. GIF tips have also recently found use in interferometric Fly-paper sensors [16–18]. In this paper the GIF tips enable demonstration of a highly effective lab-on-a-chip absorption spectroscopy platform that is compact, fiber connectorized, and does not require free-space optics or traditional lenses to create the optical path. The GIF tips have a collimated output that is transmitted longitudinally through a custom fabricated microchannel and is collected by a multimode fiber at the other end. These GIF tips can easily be incorporated into optofluidic assemblies. In addition, the GIF tip configuration can achieve 1/4 of the optical losses compared to waveguide integrated optofluidic devices such as those presented by Malic *et al.* [11].

We demonstrate that this device can allow for absorption spectroscopy to be undertaken with sample volumes ten times smaller than standard cuvettes but with similar sensitivity. This is particularly relevant for microvolume samples containing analytes such as proteins or antibodies. A proof-of-concept detection of a biologically relevant analyte, thiocyanate, in artificial human saliva, is also presented. Moreover, advanced fabrication techniques such as photolithography could be used to achieve nL volumes [7–9,11].

2. Experimental setup

2.1. GIF tips

The GIF tips used here consist of three fiber sections spliced together as shown in Fig. 1. The incoming fiber is single-mode fiber (SMF), followed by a coreless fiber (CF) segment that expands the beam. The beam then enters a graded-index fiber segment, which collimates it.

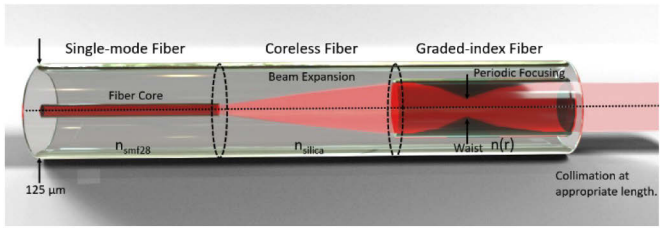

Fig. 1. Schematic of GIF tip composed of a single-mode fiber spliced to a mode expanding coreless fiber, which is spliced to a graded-index fiber. Figure adapted from [19].

Biomedical Optics EXPRESS

In this work we used Nufern GF1 single-mode fiber (NA = 0.13), Thorlabs FG125LA coreless fiber and Thorlabs GIF625 graded-index fiber. Appropriate segment lengths for minimizing the far-field divergence angle were derived (coreless segment ~ 200 µm, graded-index segment ~ 100 µm) using an optimization routine in which the coreless and graded-index fiber lengths were scanned over a large parameter space using RSOFT BeamProp. Figure 2 shows the contour plot of the far-field divergence angle (in degrees) as a function of coreless and graded-index segment lengths, that was used for optimizing the GIF tips at 532 nm. For this simulation the fundamental mode in the Nufern GF1 fiber was used. Slight variations in the beam divergence can be expected if higher-order modes are excited in the GF1 fiber. The beam divergence for the optimized GIF tip (1.31°) is much lower than for SMF28 fiber (4.6°) at $\lambda = 532$ nm. The GIF tips were fabricated by splicing 218 µm and 91 µm lengths of coreless and graded-index fiber segments, respectively, to the end of the GF1 single-mode fiber. The fabrication process involves precise thickness steel shims used in a straightforward process we have developed around a standard commercial cleaver/splicer combination. In terms of repeatability, the fabrication tolerances for the lengths of the fiber segments were approximately ±10 microns, using the steel shims that achieve the required fiber lengths when splicing together the coreless and graded-index fiber sections to the single mode fiber.

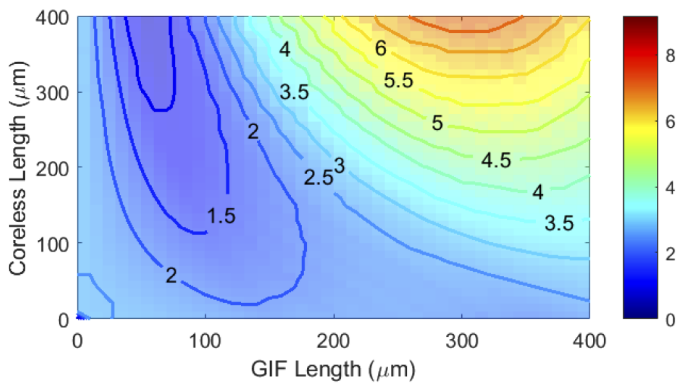

Fig. 2. Contour plot of far-field divergence angle of GIF tips (in degrees) as a function of coreless and graded-index fiber segment lengths at λ=532 nm. Fundamental mode launch in the GF1 fiber is simulated.

At this point it is worth noting that whilst GF1 and SMF28 fibers are classified and referred to as single-mode fibers, they are actually few-moded at visible wavelengths. This can have some minor influence on the beam divergence of both GIF tips and SMF fibers, although the launch conditions can be tweaked to ensure predominately fundamental mode excitation.

2.2. Microfluidic device

The microfluidic chip shown in Fig. 3 was fabricated using glass chips and precision v-grooves (sub-micron accuracy) for holding and aligning the fiber ends. These components were bonded together using NOA65 UV-curing adhesive to create a ~200 µL microchannel. To enhance single-pass absorption spectroscopy measurements within the microfluidic chip, the fabricated GIF tip (excitation fiber) was aligned to a Thorlabs M137L03 200 µm core multimode fiber (collection fiber) using the two spaced v-grooves (127 µm pitch). After precise insertion of the fibers into the v-grooves, the fibers were fixed using the UV-curable optical adhesive. The length of the channel between the excitation fiber and the collection fiber defines the optical path length which in this case was 10.0 mm. To assess the performance of the optofluidics cuvette (volume

Biomedical Optics EXPRESS

3.5 mL) in a standard setup using the same input source as the microfluidic device as shown in Fig. 4(a).

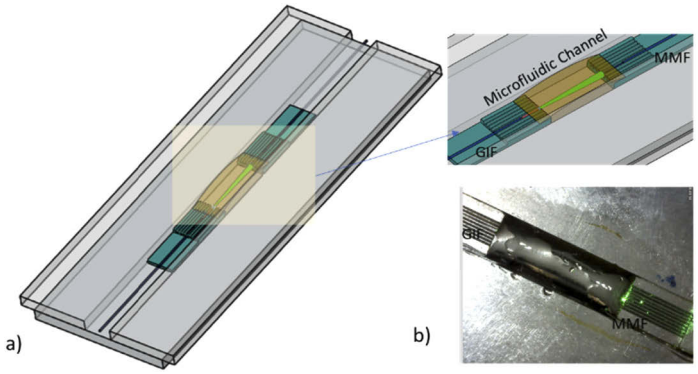

Fig. 3. (a) Device design showing microfluidic channel and GIF tip aligned to MMF within v-grooves (b). Close-up of channel.

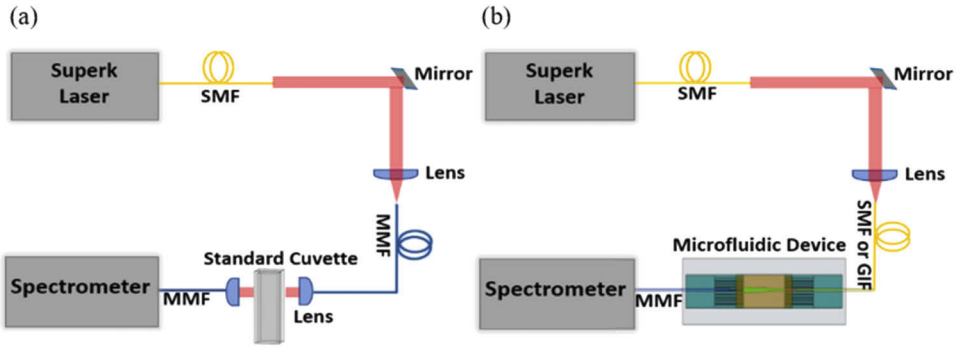

Fig. 4. Experimental setup for absorption measurements with (a) standard cuvette and (b) microfluidic device.

2.3. Absorption spectroscopy setup

To measure absorption spectra, a broadband supercontinuum laser (YSL Photonics SC-OEM) was used as the excitation source in addition to a monochromator (iHR550, Horiba, Japan) equipped with three different gratings; 600, 1200, and 2400 mm^{-1} and a cooled CCD (Synapse 2048 pixels, Horiba, Japan). The Horiba iHR550 monochromator was used for detection in both the standard cuvette and microfluidic device setups. The experimental setup is illustrated in Fig. 4 for the (a) 10.00 mm width standard cuvette and the (b) custom microfluidic device. The standard cuvette setup required traditional lenses to collimate the output beam of the MMF (excitation fiber) and to focus the beam in the receiving MMF (collection fiber). In the case of the microfluidic device, the collimated beam is directed longitudinally through the microchannel and collected by the multimode fiber at the other end. The standard cuvette and GIF-enabled microfluidic chips were compared for a range of analytes including red food colour dye (Ponceau 4R Food Color), thiocyanate in water and in artificial human saliva.

The artificial human saliva was prepared based on the composition of the SAGF medium with minor modification [20]. This involved mixing sodium chloride (125 mg), potassium chloride (964 mg), calcium chloride dihydrate (228 mg), potassium phosphate monobasic (655 mg), urea

Biomedical Optics EXPRESS

(200 mg), sodium bicarbonate (631 mg), disodium sulfate decahydrate (763 mg) and ammonium chloride (178 mg) in 1 L of MilliQ water. Different amounts of sodium thiocyanate were added to prepare a series of thiocyanate concentrations. For this experiment the beam divergence of the GIF and SMF were measured using an Ophir Spiricon silicon-based CCD camera. To ensure predominantly single-mode operation the launch conditions were tweaked for the SMF fibers. To study the coupling and transmission losses between SMF-MMF and GIF-MMF fibers as a function of channel length, an optical power meter (Thorlabs S120C, PM100D) was used.

3. Results and discussion

In this section we demonstrate the operation of the microfluidic device using a simple solution of red color dye. Absorption spectroscopy is then demonstrated for iron (III) thiocyanate $Fe(SCN)^{2+}$ prepared in water. Finally, the sensing platform is shown for the specific application of detecting the thiocyanate biomarker in artificial human saliva.

3.1. Red color dye

The absorption of the red food color dye at its absorption peak of 501 nm is shown in Fig. 5 as a function of dye concentration (5 µM to 33 µM) for both the standard cuvette and the custom GIF-enabled microfluidic chip. The absorption spectrum measured using the supercontinuum source is given for all concentrations in the inset of Fig. 5.

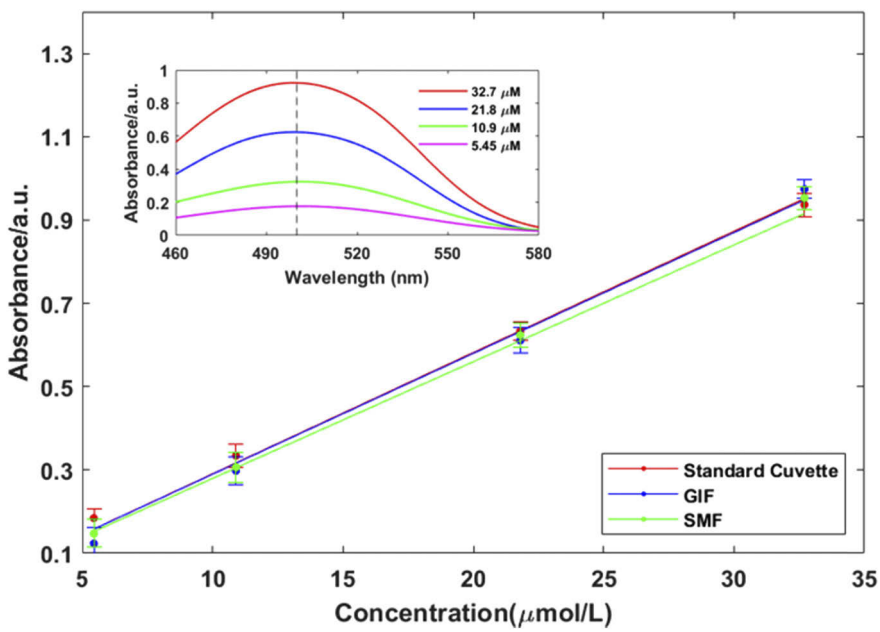

Fig. 5. Plot of absorbance at 501 nm of red color dye for a standard cuvette (A = 0.029C) and the microfluidics chip with either GIF tip (A = 0.029C) or SMF fiber (A = 0.029C). The inset shows the absorption spectra of concentrations ranging from 5.45 µmol/L to 32.7 µmol/L.

To mitigate the effect of laser instability, the transmitted power I for each measurement is normalized to the power recorded prior to filling the microchannel with the analyte. The absorbance measurements at each concentration, A, were obtained by taking the ratio of the normalized transmitted power I to the power I_o recorded in absence of the analyte of interest. The calibration curves in Fig. 5 clearly show the linearity of absorbance with dye

Biomedical Optics EXPRESS

concentration, according to the Beer-Lambert law, Eq. (1). The molar absorptivity value is $\varepsilon \approx 28,891\ L.mol^{-1}cm^{-1}$, which is in agreement with literature [21]. The quantitative analysis shows the ability to reproduce linearity using a microfluidic device with only ~200 µL of solution compared with the 3.5 mL standard cuvette, while maintaining the same interaction length. This is particularly noteworthy given that only small sample volumes are commonly accessible in point-of-care diagnostics. Although the microfluidic device absorbance results are comparable when using the standard SMF28 fiber and the GIF tip, the significantly higher beam divergence of SMF means there is lower collection efficiency at the MMF. For this reason, higher power is required in the SMF compared to the GIF tip to achieve similar signal to noise ratios. The far-field divergence angle of both fibers is shown in Fig. 6(a). The GIF tip presents a near-collimated beam of 1.31° far-field divergence angle, which is approximately 4× lower than the 4.6° far-field divergence angle for SMF28 fiber at 532 nm. Figure 6(b) compares the diverging beam radius of the SMF and the GIF tip as a function of propagation distance at wavelengths of 532 nm and 650 nm. As predicted, the beam divergence is relatively insensitive to wavelength changes of the order of ~100 nm.

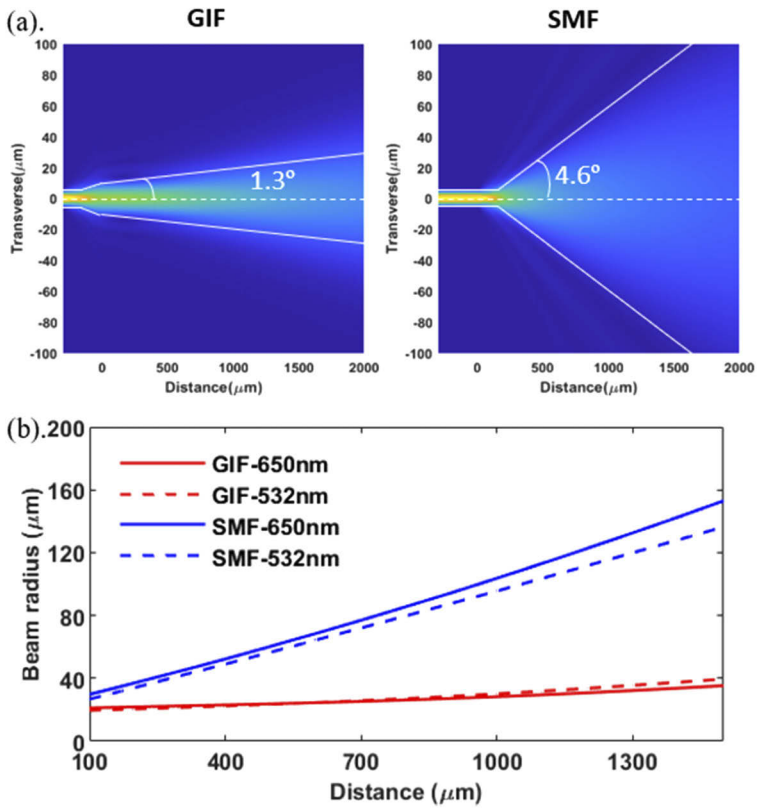

Fig. 6. (a). The beam divergence angle of SMF28 and the GIF tip (coreless fiber segment = 218 µm and graded-index segment = 91 µm). (b) Measured beam radius of SMF28 (blue curves) and GIF tip (red curves) as a function of propagation distance at 532 nm and 650 nm.

The comparison of SMF-MMF and GIF-MMF coupling efficiencies is shown in Fig. 7. The graph shows that for a fixed distance between the excitation and collection fibers (10.0 mm) the optical losses can be 15× lower when using the GIF tip fiber. This effectively means the GIF setup could be used for significantly longer channels for a given permissible insertion loss. In

Biomedical Optics EXPRESS

addition, the GIF setup has 4× less optical losses compared to waveguide integrated optofluidic devices presented by for example Malic *et al*. [11].

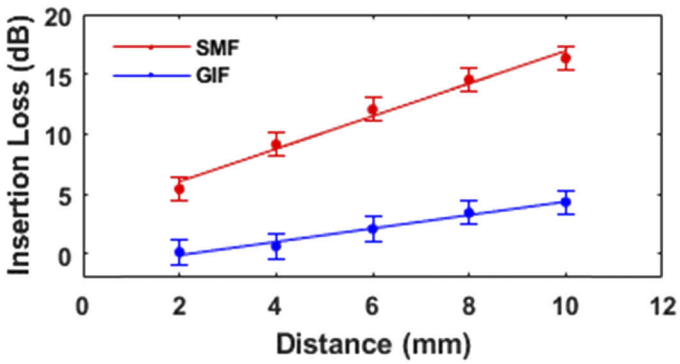

Fig. 7. Measured insertion losses of GIF-MMF and SMF-MMF configurations.

The low insertion losses also mean that lower power can be used for a given channel length, avoiding potential issues such as bleaching of the sample when higher powers are required. This shows the significant benefits of using GIF tips in fiber connectorized lab-on-a-chip spectroscopic applications.

3.2. Thiocyanate in water

To further demonstrate this optofluidic setup, we show that it can be used for detection of biologically-relevant analytes such as thiocyanate. Thiocyanate (SCN^-) was chosen as it is of particular interest in medical diagnostics [22], because it is a detoxification product of cancers and an indicator of oral health including exposure to passive smoking [23]. The complexation reaction between the Fe (III) ions and SCN^- ligands (non-metal) forms a red-orange color compound, $Fe(SCN)^{2+}$, which allows for color techniques such as absorption spectroscopy to be used for its detection Absorption measurements at 480 nm (close to the 460 nm absorption peak of $Fe(SCN)^{2+}$ but far enough away from the supercontinuum wavelength cut-off) were performed using the same setup as before, mixing in 1:1 ratio by volume various SCN^- concentrations (50 µM to 410 µM) with a 26.4 mM concentration of Fe(III)), and a 1:1 mixture of the Fe(III) solution and water was used as the reference. Note that after mixing the SCN^- solution with the Fe(III) solution, fading of the color over time occurs [24]. To avoid this the absorbance measurements were performed immediately after mixing the two reagents. The uncertainty in the measurements was determined from the standard deviation of 10 measurements taken of the spectrum over a duration of 100 seconds. Figure 8 shows the absorption spectra and the absorbance as a function of the SCN^-concentration for the three configurations described, with the results showing comparable linearity according to the Beer-Lambert Law. Based on the Beer-lambert law the molar absorptivity of $Fe(SCN)^{2+}$ at the wavelength of 480 nm can be determined as, $\varepsilon \approx 2389\ L.mol^{-1}cm^{-1}$. This is lower than the reported value in the literature (i.e. $\lambda = 480$ nm, $\varepsilon = 3914$ L. mol^{-1} cm^{-1}; $\lambda = 500$ nm, $\varepsilon = 2900$ L.mol^{-1} cm^{-1} with ionic strength being 0.5) [25], most likely due to the lower ionic strength in our solutions (i.e. 0.1) compared to that used in the literature.

3.3. Thiocyanate in artificial saliva

We also explore the GIF tip enabled optofluidic setup for thiocyanate detection in a more complicated sample matrix other than water, artificial saliva, underpinning its potential for

Biomedical Optics EXPRESS

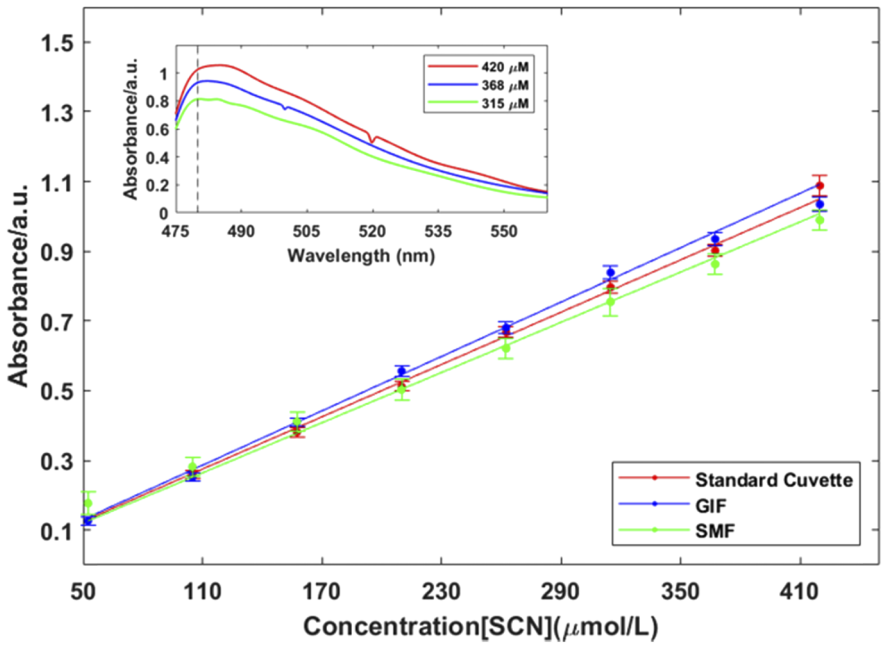

Fig. 8. Plot of absorbance at 480 nm for $Fe(SCN)^{2+}$ solution as a function of SCN^- concentration in water for standard cuvette (A = 0.0025C) and for the microfluidic chip with either GIF (A = 0.0026C) or SMF (A = 0.0024C). The absorption spectra (using the supercontinuum source) are plotted for concentrations ranging from 315 μmol/L to 420 μmol/L.

point-of-care diagnosis. The results were therefore repeated by preparing the $Fe(SCN)^{2+}$ solution in artificial saliva.

The results in Fig. 9 show the linearity and comparable absorbance at 480 nm for the SCN^- in water and artificial saliva. This successful demonstration shows that it is possible to extend the tests of these microfluidic chips to saliva, which is a typical biological sample where SCN^- concentrations range from 0.5–2 mM in non-smokers and up to 6 mM in smokers [26]. The limit of detection (LOD) of this simple and practical optofluidic device is determined by the

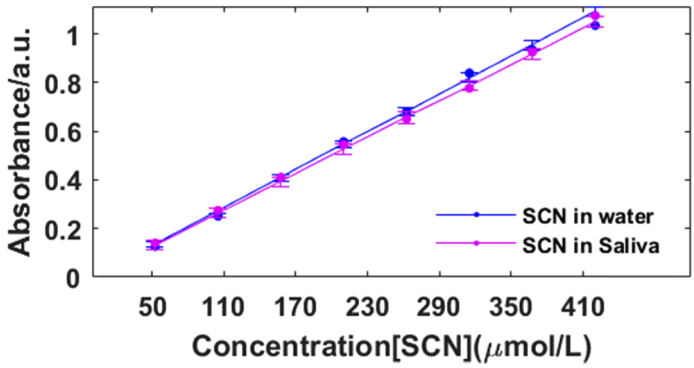

Fig. 9. Plot of absorbance at 480 nm as a function of SCN^- solution in artificial saliva (A = 0.0025C) and in water (A = 0.0026C) for the GIF setup.

Biomedical Optics EXPRESS

minimum reliably detected concentration of SCN^- in artificial saliva which is 16.2 μM. Salivary thiocyanate could for instance be used to evaluate the influence of passive smoking on public health or to detect thyroid gland malfunction [22]. Although other techniques exist to detect SCN^- such as surface-enhanced Raman spectroscopy using droplet microfluidic chips [27], and chromatography mass spectroscopy [28], we present a simple and compact fiber-coupled platform to achieve detection, with the technique presented being extendable to cavity-enhanced approaches which would further enhance sensitivity.

4. Conclusion

In summary we have demonstrated a microfluidic device which shows identical performance to standard cuvettes for absorption spectroscopy but renders a 10-fold reduction in the sample volume. This is enabled by using graded-index fiber tips which collimate the output of an optical fiber and could allow for longer channel lengths. The GIF tips are shown to allow for a significant reduction in insertion loss when compared with the microfluidic chips using standard SMF. The simple and practical microfluidic chips are shown to detect down to 50 μM concentration of SCN^- in artificial saliva, which is more than sufficient for the quantitative measurement of SCN^- in saliva for the identification of irregularities in saliva and the monitoring of oral health. Moreover, the microfluidic devices demonstrated in this paper could be integrated for lab-on-a-chip devices or implemented for highly sensitive cavity-enhanced absorption technologies.

Funding

Australian Research Council (IH150100028).

Acknowledgements

K. Gill, N. Riesen, C. Priest and D. Lancaster acknowledge financial support from ULVAC Inc., and the Australian Research Council Integrated Device for End-User Analysis at Low Levels Research (IDEAL) Hub (IH150100028).

Disclosures

The authors declare that there are no conflicts of interest related to this article.

References

1. P. Minzioni, R. Osellame, C. Sada, S. Zhao, F. Omenetto, K. B. Gylfason, T. Haraldsson, Y. Zhang, A. Ozcan, and A. Wax, "Roadmap for optofluidics," J. Opt. **19**(9), 093003 (2017).
2. C. Song and S. H. Tan, "A Perspective on the Rise of Optofluidics and the Future," Micromachines **8**(5), 152 (2017).
3. D. Psaltis, S. R. Quake, and C. Yang, "Developing optofluidic technology through the fusion of microfluidics and optics," Nature **442**(7101), 381–386 (2006).
4. M. Savoini, P. Biagioni, L. Duò, and M. Finazzi, "All-optical subdiffraction multilevel data encoding onto azo-polymeric thin films," Opt. Lett. **34**(6), 761–763 (2009).
5. G. Holzner, F. H. Kriel, and C. Priest, "Pillar cuvettes: capillary-filled, microliter quartz cuvettes with microscale path lengths for optical spectroscopy," Anal. Chem. **87**(9), 4757–4764 (2015).
6. F. H. Kriel and C. Priest, "Influence of sample volume and solvent evaporation on absorbance spectroscopy in a microfluidic "pillar-cuvette"," Anal. Sciences **32**, 103–108 (2016).
7. S. R. Neil, C. M. Rushworth, C. Vallance, and S. R. Mackenzie, "Broadband cavity-enhanced absorption spectroscopy for real time, in situ spectral analysis of microfluidic droplets," Lab Chip **11**(23), 3953–3955 (2011).
8. C. M. Rushworth, G. Jones, M. Fischlechner, E. Walton, and H. Morgan, "On-chip cavity-enhanced absorption spectroscopy using a white light-emitting diode and polymer mirrors," Lab Chip **15**(3), 711–717 (2015).
9. A. Nitkowski, L. Chen, and M. J. Lipson, "Cavity-enhanced on-chip absorption spectroscopy using microring resonators," Opt. Express **16**(16), 11930–11936 (2008).
10. S. M. Ball, J. M. Langridge, and R. Jones, "Broadband cavity enhanced absorption spectroscopy using light emitting diodes," Chem. Phys. Lett. **398**(1-3), 68–74 (2004).
11. L. Malic and A. G. Kirk, "Integrated miniaturized optical detection platform for fluorescence and absorption spectroscopy," Sens. Actuators, A **135**(2), 515–524 (2007).

Biomedical Optics EXPRESS

12. C. Wang, Y. Mao, C. Fang, Z. Tang, Y. Yu, and B. Qi, "Analytical method for designing gradient-index fiber probes," Opt. Eng. **50**(9), 094202 (2011).
13. S. Bi, C. Wang, J. Zhu, Z. Yuan, Y. Yu, S. Valyukh, and A. Asundi, "Influence of no-core fiber on the focusing performance of an ultra-small gradient-index fiber probe," Opt. Laser Eng. **107**, 46–53 (2018).
14. D. Lorenser, X. Yang, and D. D. Sampson, "Accurate modeling and design of graded-index fiber probes for optical coherence tomography using the beam propagation method," IEEE Photonics J. **5**(2), 3900015 (2013).
15. M. Zickar, W. Noell, C. Marxer, and N. de Rooij, "MEMS compatible micro-GRIN lenses for fiber to chip coupling of light," Opt. Express **14**(10), 4237–4249 (2006).
16. C. Wang, J. Sun, C. Yang, B. Kuang, D. Fang, and A. Asundi, "Research on a novel Fabry–Perot interferometer model based on the ultra-small gradient-index fiber probe," Sensors **19**(7), 1538 (2019).
17. Y. Zhang, Y. Li, T. Wei, X. Lan, Y. Huang, G. Chen, and H. Xiao, "Fringe visibility enhanced extrinsic Fabry–Perot interferometer using a graded index fiber collimator," IEEE Photonics J. **2**(3), 469–481 (2010).
18. B. Du, X. Xu, J. He, K. Guo, W. Huang, F. Zhang, M. Zhang, and Y. Wang, "In-Fiber collimator-based Fabry-Perot interferometer with enhanced vibration sensitivity," Sensors **19**(2), 435 (2019).
19. N. Riesen, N. Phillips, C. Priest, L. V. Nguyen, and D. Lancaster, "Lensed GRIN fiber-optic Fabry-Perot interferometers," *Frontiers in Optics* JTu7D, JTu7D.4 (2020).
20. J.-Y. Gal, Y. Fovet, and M. Adib-Yadzi, "About a synthetic saliva for in vitro studies," Talanta **53**(6), 1103–1115 (2001).
21. K. Bevziuk, A. Chebotarev, D. Snigur, Y. Bazel, M. Fizer, and V. Sidey, "Spectrophotometric and theoretical studies of the protonation of Allura Red AC and Ponceau 4R," J. Mol. Struct. **1144**, 216–224 (2017).
22. M. F. Erdoğan, "Thiocyanate overload and thyroid disease," Biofactors **19**(3-4), 107–111 (2003).
23. A. Phonchai, T. Srisukpan, S. Riengrojpitak, P. Wilairat, and R. Chantiwas, "Simple and rapid screening of the thiocyanate level in saliva for the identification of smokers and non-smokers by capillary electrophoresis with contactless conductivity detection," Anal. Methods **8**(25), 4983–4990 (2016).
24. K. de Berg, M. Maeder, and S. Clifford, "A new approach to the equilibrium study of iron (III) thiocyanates which accounts for the kinetic instability of the complexes particularly observable under high thiocyanate concentrations," Inorg. Chim. Acta **445**, 155–159 (2016).
25. H. S. Frank and R. L. Oswalt, "The stability and light absorption of the complex ion $FeSCN^{++}$," J. Am. Chem. Soc. **69**(6), 1321–1325 (1947).
26. C. V. Kalburgi, K. L. Naik, M. V. Kokatnur, and S. Warad, "Estimation and correlation of salivary thiocyanate levels in healthy and different forms of tobacco users having chronic periodontitis: A cross-sectional biochemical study," Contemp. Clin. Dent. **5**(2), 182 (2014).
27. L. Wu, Z. Wang, S. Zong, and Y. Cui, "Rapid and reproducible analysis of thiocyanate in real human serum and saliva using a droplet SERS-microfluidic chip," Biosens. Bioelectron. **62**, 13–18 (2014).
28. R. K. Bhandari, R. P. Oda, S. L. Youso, I. Petrikovics, V. S. Bebarta, G. A. Rockwood, and B. A. Logue, "Simultaneous determination of cyanide and thiocyanate in plasma by chemical ionization gas chromatography mass-spectrometry (CI-GC-MS)," Anal. Bioanal. Chem. **404**(8), 2287–2294 (2012).